J. Fluid Mech. (2024), *vol*. 979, A33, doi:10.1017/jfm.2023.1089

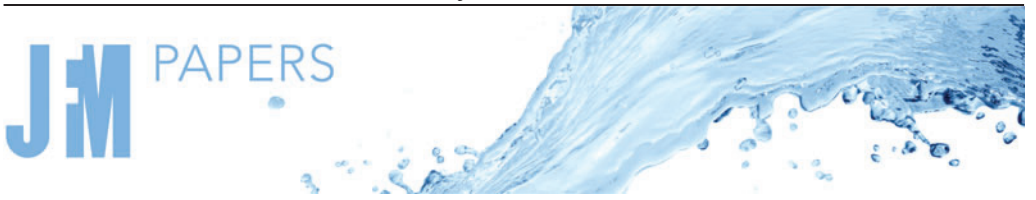

On the time scales of spectral evolution of nonlinear waves

Ashleigh Simonis[1], **Alexander Hrabski**[1] **and Yulin Pan**[1],†

[1]Department of Naval Architecture and Marine Engineering, University of Michigan, Ann Arbor, MI 48109, USA

(Received 22 May 2023; revised 15 December 2023; accepted 17 December 2023)

As presented in Annenkov & Shrira (*Phys. Rev. Lett.*, vol. 102, 2009, 024502), when a surface gravity wave field is subjected to an abrupt perturbation of external forcing, its spectrum evolves on a 'fast' dynamic time scale of $O(\varepsilon^{-2})$, with ε a measure of wave steepness. This observation poses a challenge to wave turbulence theory that predicts an evolution with a kinetic time scale of $O(\varepsilon^{-4})$. We revisit this unresolved problem by studying the same situation in the context of a one-dimensional Majda–McLaughlin–Tabak equation with gravity wave dispersion relation. Our results show that the kinetic and dynamic time scales can both be realised, with the former and latter occurring for weaker and stronger forcing perturbations, respectively. The transition between the two regimes corresponds to a critical forcing perturbation, with which the spectral evolution time scale drops to the same order as the linear wave period (of some representative mode). Such fast spectral evolution is mainly induced by a far-from-stationary state after a sufficiently strong forcing perturbation is applied. We further develop a set-based interaction analysis to show that the inertial-range modal evolution in the studied cases is dominated by their (mostly non-local) interactions with the low-wavenumber 'condensate' induced by the forcing perturbation. The results obtained in this work should be considered to provide significant insight into the original gravity wave problem.

Key words: surface gravity waves

1. Introduction

Wave turbulence theory describes the statistical properties of ensembles of weakly nonlinear interacting waves, with rich applications in many physical contexts,

† Email address for correspondence: yulinpan@umich.edu

e.g. ocean waves (Zakharov & Filonenko 1967; Nazarenko & Lukaschuk 2016), acoustics (L'vov *et al.* 1997), magnetohydrodynamics (Galtier *et al.* 2000), quantum turbulence (Nazarenko & Onorato 2006) and others. The centrepiece of wave turbulence theory is a wave kinetic equation (WKE), which describes the time evolution of the wave action spectrum as an integral over wave–wave interactions. The WKE yields a stationary Kolmogorov–Zakharov power-law solution associated with a constant flux, which has been observed in many wave systems.

Quantitative validations of the WKE and its predictions in different physical contexts have been a prominent topic in the wave turbulence community for decades. These studies include extensive numerical and experimental validations of the spectral slope and energy flux (or Kolmogorov constant) of the Kolmogorov–Zakharov solutions (e.g. Pan & Yue 2014; Falcon & Mordant 2022; Hrabski & Pan 2022; Zhang & Pan 2022*a*; Zhu *et al.* 2023), numerical validation of the initial spectral evolution predicted by the WKE (e.g. Banks *et al.* 2022; Zhu *et al.* 2022) and rigorous mathematical justification of the WKE (e.g. Buckmaster *et al.* 2021; Deng & Hani 2021, 2023). Although successes in verifying the WKE have been reported in many cases, situations where WKE predictions fail have also been identified, such as circumstances associated with finite-size effects (e.g. L'vov & Nazarenko 2010; Hrabski & Pan 2020; Zhang & Pan 2022*b*), coherent structures in the field (e.g. Rumpf, Newell & Zakharov 2009) and the strong turbulence regime (e.g. Chibbaro, De Lillo & Onoroto 2017).

In spite of the significant advancement in understanding the WKE, there exists a series of relevant studies on surface gravity waves that remain largely unexplained. A representative work of this series is the paper by Annenkov & Shrira (2009), which considers the spectral evolution when a stationary gravity wave field is subjected to an abrupt perturbation of external wind forcing. According to the WKE of gravity waves, in the form of $\partial n/\partial t \sim n^3$ with $n \sim \varepsilon^2$ the wave action spectrum, one would expect an evolution with the kinetic time scale of $O(\varepsilon^{-4})$. However, simulations of the dynamic equation, specifically the Zakharov equation (Zakharov 1968), show a faster evolution with a dynamic time scale of $O(\varepsilon^{-2})$. We remark that this 'fast' spectral evolution refers to the scaling of time scale with ε, instead of the evolution rate in its absolute value. Although with some uncertainties in measurement, the 'fast' spectral evolution is also observed in wave-tank experiments (e.g. Autard 1995; Waseda, Toba & Tulin 2001) and field studies (van Vledder & Holthuijsen 1993) when the wind exhibits a sudden change in speed or direction, as well as numerical simulations for the initial evolution of some wave spectra (Dyachenko *et al.* 2003). In a study by Annenkov & Shrira (2018), an attempt is made in explaining the fast spectral evolution using the so-called generalised WKE, but only limited success is achieved. This unexplained issue is concerning since the WKE of surface gravity waves (also known as Hasselmann's kinetic equation; Hasselmann 1962) is currently used in modern wave modelling codes whose reliability is pertinent to weather forecasting, climate modelling and navigation (Janssen 2004).

In this paper, we revisit the spectral evolution problem in the context of the one-dimensional (1-D) Majda–McLaughlin–Tabak (MMT) equation with gravity wave dispersion relation. The MMT model is favourable in the sense that it captures the essential dynamics of wave turbulence while being exempt from the complexities associated with surface gravity waves. One of these critical complexities is the existence of quasi-resonant three-wave interactions in surface gravity waves (an issue under investigation in the field), which can affect the observed spectral evolution time scale. The mathematical procedure to remove the quadratic terms in deriving the WKE of surface gravity waves is also not fully justified for finite wave steepness ε. In addition, with a 1-D model, we are able

to perform large numbers of ensemble simulations, with which the statistical properties can be reliably computed through ensemble averages. We conduct the study and analysis closely following Annenkov & Shrira (2009), i.e. with numerical set-ups and evaluation of properties as consistent as possible, except using the 1-D MMT model.

For a given stationary wave field, we show that evolution with kinetic and dynamic time scales can be observed for weaker and stronger forcing perturbations, respectively. The transition from the former to the latter regime corresponds to a forcing perturbation that triggers a spectral evolution time scale comparable to the linear time scale, i.e. the wave period of some representative mode, violating the basis of the WKE. We further show, through a study varying the energy of the base stationary wave field, that this violation of time-scale separation is primarily a result of the spectrum far from the stationary state after a sufficiently strong forcing perturbation is applied, rather than the increase of overall nonlinearity level of the wave field. We finally develop a set-based interaction analysis, which allows us to understand that the spectral evolution for modes in the inertial range is predominantly governed by their (mostly non-local) interactions with the low-wavenumber condensate (or regions sufficiently filled with energy) induced by the forcing perturbation.

2. Methodology

2.1. *The MMT model*

We study the evolution of random wave fields through the 1-D MMT equation (Majda, McLaughlin & Tabak 1997), which is a family of nonlinear dispersive wave equations widely used to study wave turbulence problems (e.g. Cai *et al.* 1999; Zakharov, Pushkarev & Dias 2001; Chibbaro *et al.* 2017; Hrabski & Pan 2022):

$$\mathrm{i}\frac{\partial \psi}{\partial t} = |\partial_x|^{\alpha}\psi + \lambda|\partial_x|^{\beta/4}(||\partial_x|^{\beta/4}\psi|^2|\partial_x|^{\beta/4}\psi), \tag{2.1}$$

where $\psi(x, t)$ is a field taking complex values. The parameter β controls the nonlinearity formulation and α controls the dispersion relation $\omega(k) = |k|^{\alpha}$ with ω the frequency and k the wavenumber. Here $\lambda = -1$ and 1 represent the focusing (defocusing) nonlinearity, respectively (Cai *et al.* 2001). The MMT equation (2.1) conserves both the total Hamiltonian and wave action. In our study, we use $\alpha = 1/2$ to mimic the dispersion of surface gravity waves, and use $\beta = 0$ for convenience which is consistent with a portion of the original study of the MMT equation (Majda *et al.* 1997) and is widely used in other studies (e.g. Cai *et al.* 1999; Rumpf & Newell 2013; Rumpf & Sheffield 2015). We note that although $\beta = 0$ is not entirely representative of surface gravity waves, the primary conclusion of the paper does not depend on a specific choice of β. We present the results for the defocusing case ($\lambda = 1$) in the main paper, and those for the focusing case in Appendix B, with both cases exhibiting similar physics regarding the spectral evolution time scales.

From a standard wave turbulence consideration, a statistical description of the wave field can be obtained by defining the wave action spectrum $n_k = \langle|\hat{\psi}_k|^2\rangle$, with $\hat{\psi}_k$ the Fourier transform of ψ and the angle brackets denoting an ensemble average. Under conditions of weak nonlinearity, random phases and infinite domain, the time evolution of n_k is governed by the WKE (for $\beta = 0$):

$$\frac{\partial n_k}{\partial t} = 4\pi \int (n_1 n_2 n_3 + n_1 n_2 n_k - n_1 n_3 n_k - n_2 n_3 n_k) \times \delta(\omega_1 + \omega_2 - \omega_3 - \omega)\delta(k_1 + k_2 - k_3 - k)\,\mathrm{d}k_1\,\mathrm{d}k_2\,\mathrm{d}k_3, \tag{2.2}$$

where δ is the Dirac delta function. According to (2.2), the spectrum evolves with a kinetic time scale, i.e. n_k experiences significant change with a time scale of $O(\varepsilon^{-4})$, and $\partial n_k/\partial t \sim O(\varepsilon^6)$ over the evolution, with $\varepsilon \sim \sqrt{n_k}$ a measure of wave steepness. Hereafter, we refer to these relations as kinetic scaling in this paper, which is in contrast to the dynamic scaling of a time scale of $O(\varepsilon^{-2})$ and $\partial n_k/\partial t \sim O(\varepsilon^4)$ that one can directly obtain from (2.1).

2.2. *Numerical procedure*

We simulate (2.1) with 4096 modes (before de-aliasing) on a periodic domain of size $L = 2\pi$, with the addition of forcing and dissipation terms. The forcing is in white-noise form, given by

$$F = \begin{cases} F_r + \mathrm{i}F_i, & 4 \le k \le 13, \\ 0, & \text{otherwise}, \end{cases} \tag{2.3}$$

with F_r and F_i independently drawn from a Gaussian distribution $\mathcal{N}(0, \sigma^2)$. The dissipation is introduced with the addition of two hyperviscosity terms

$$\left.\begin{aligned} D_1 &= \begin{cases} -\mathrm{i}\nu_1\hat{\psi}_k, & k \ge 900, \\ 0, & \text{otherwise}, \end{cases} \\ D_2 &= \begin{cases} -\mathrm{i}\nu_2\hat{\psi}_k, & k \le 4, \\ 0, & \text{otherwise}, \end{cases} \end{aligned}\right\} \tag{2.4}$$

at small and large scales, respectively. Since the MMT model supports the inverse cascade, it is necessary to use large-scale dissipation to avoid energy accumulation at large scales. The dissipation coefficients are fixed to be $\nu_1 = 1 \times 10^{-14}(k - 900)^8$ and $\nu_2 = 3k^{-4}$ for all numerical experiments. The numerical schemes used for the simulation are discussed in detail in previous papers (Hrabski & Pan 2020, 2022).

In order to reproduce the physical scenario as in Annenkov & Shrira (2009), we perform the simulation with two stages. In stage 1, we simulate (2.1) with (2.3) and (2.4) using $\sigma = \sigma_0$ for sufficient time to reach a stationary wave field (and spectrum), starting from an initial spectrum that exponentially decays in $|k|$. In stage 2, we add a perturbation $\Delta\sigma$ to the forcing magnitude (leading to $\sigma = \sigma_0 + \Delta\sigma$) and study how the spectrum evolves subject to the perturbation. In both stages, we use a time step $\Delta t = 0.012$. For the main cases studied in this paper, we consider the stationary state obtained with forcing $\sigma_0 = 0.004$ in stage 1, and consider forcing perturbations $\Delta\sigma \in [0.033, 1.461]$ in stage 2 that is sufficient to cover the physical regimes of our interest. The process is simulated with an ensemble of 65 000 simulations with different random seeds in the forcing, and all statistical results related to n_k presented below are obtained directly from the average over the whole or part of the ensemble that is statistically convergent.

3. Results

Figure 1 shows the evolution of a spectrum in a typical case with $\sigma_0 = 0.004$ and $\Delta\sigma = 0.033$. We see that a stationary power-law spectrum forms at the end of stage 1, which serves as the base state of the problem. As a forcing perturbation is excited in stage 2, the forcing scales (as well as scales slightly larger than that) first experience an abrupt growth, forming a condensate at large scales. The growth is then propagated to smaller scales,

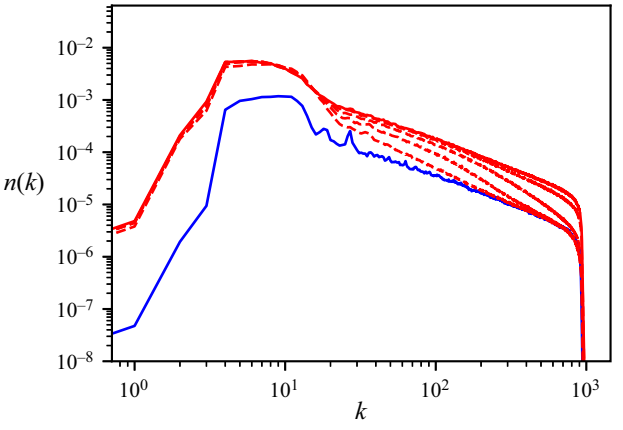

Figure 1. A typical case of the evolution of wave action spectrum, where $n(k, 0)$ (solid blue) and $n(k, t_f)$ (solid red) represent the stationary spectra before the forcing perturbation (stage 1) and after sufficient evolution with forcing perturbation applied (stage 2). The intermediate spectra in the evolution between $n(k, 0)$ and $n(k, t_f)$ are plotted (dashed red).

which eventually fill in the full spectral range and form the final stationary power-law spectrum. We note that such behaviour regarding the propagation of growth is closely related to the fact that (2.1) under selected values of α and β is an infinite-capacity system (Nazarenko 2011; Newell & Rumpf 2011). Hereafter, for simplicity, we assign time $t = 0$ to the stationary state before a forcing perturbation is applied, and $t = t_f$ to the time when the final stationary state is formed. We measure the wave steepness of each state as $\varepsilon = \sqrt{E_L}$ with E_L the linear energy (or Hamiltonian) of the system. Accordingly, we use ε_0 and ε_f as the wave steepness at $t = 0$ and $t = t_f$. We note that this definition of ε is consistent with that in Annenkov & Shrira (2009) with the additional factor of constant peak wavenumber k_p omitted in our definition.

We are interested in the growth rate in the transient period in stage 2, based on which we can evaluate $\partial n_k/\partial t$ and the associated scaling with wave steepness. For this purpose, we follow Annenkov & Shrira (2009) to measure $\partial n_k/\partial t$ for a given mode k using data over the interval of 5 %–40 % of the full modal growth. More specifically, if we define a normalised wave action spectrum $\tilde{n}(k, t) = (n(k, t) - n(k, 0))/(n(k, t_f) - n(k, 0))$, we can then measure $\partial \tilde{n}_k/\partial t$ over the range of $\tilde{n}_k \in [5\,\%, 40\,\%]$ via a least-squares fit, and then scale back to compute $\partial n_k/\partial t$. Figure 2 shows the evolution of $\tilde{n}(k, t)$ for three selected modes in the inertial range, as well as the growth rate evaluated using the [5 %, 40 %] interval. We note that each modal growth exhibits a short exponential regime followed by an algebraic regime, and that our [5 %, 40 %] covers the growth predominantly in the algebraic regime. Furthermore, we have tested that the obtained results are not sensitive to a variation of bounds of the interval to [25 %, 60 %] and likely more. Therefore, the evaluated growth rate over the chosen interval [5 %, 40 %] is robust to capture the typical spectral growth after the forcing perturbation is imposed.

3.1. *Scaling of spectral growth rate with ε*

To evaluate the scaling of $\partial n_k/\partial t$ with the wave steepness ε, we use the final-state $\varepsilon = \varepsilon_f$ as a representative value of the wave steepness for the case (cf. Annenkov & Shrira 2009). Figure 3 shows $\partial n_k/\partial t$ of three modes in the inertial range for a broad range of $\varepsilon \in [0.022, 0.124]$, obtained from 22 cases with $\Delta\sigma \in [0.033, 1.461]$ starting from a base

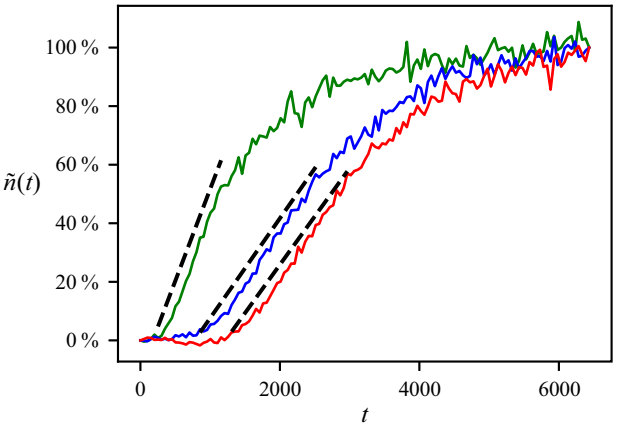

Figure 2. A typical case of the evolution of modal wave action at three wavenumbers $k = 150$ (solid green), $k = 500$ (solid blue) and $k = 800$ (solid red) in the inertial range. The growth rates $\partial\tilde{n}_k/\partial t$ measured over the range of $\tilde{n}_k \in [5\,\%, 40\,\%]$ are indicated (dashed).

state with $\varepsilon_0 = 0.010$ resulting from $\sigma_0 = 0.004$. As we see in figure 3, the kinetic scaling $\partial n_k/\partial t \sim O(\varepsilon^6)$ is realised in the range of $\varepsilon \lesssim 0.05$, corresponding to small $\Delta\sigma$ with $\Delta\sigma \lesssim 0.36$. For larger forcing perturbations, we find dynamic scaling in the range of $\varepsilon \gtrsim 0.05$. We remark that in the previous work for gravity waves (Annenkov & Shrira 2009), only dynamic scaling is observed. This is possibly due to those studies only being conducted for strong forcing perturbations, or other reasons that we will leave for future study.

We next investigate why the 'fast' dynamic scaling becomes relevant for the spectral evolution, a critical question that is not answered in previous works (e.g. Annenkov & Shrira 2006, 2009, 2018). The realisation of dynamic scaling indicates that the WKE (2.2) (or more generally, wave turbulence theory) must break down. One situation in which this could happen is a violation of time-scale separation, i.e. when the nonlinear modal time scale becomes comparable to the linear modal time scale. In particular, the linear time scale of a mode is given by the modal wave period:

$$\tau_{lin} = \frac{2\pi}{\omega}. \tag{3.1}$$

The nonlinear time scale can be computed in our case as the spectral evolution time scale:

$$\tau_{nl} = \frac{n_k}{\dfrac{\partial n_k}{\partial t}}, \tag{3.2}$$

with $\partial n_k/\partial t$ evaluated from our numerical data. Hereafter, we also use the terminology 'spectral evolution time scale' which is somewhat more illuminating than 'nonlinear time scale'. In addition, we note that in many cases (e.g. Newell, Nazarenko & Biven 2006; Newell & Rumpf 2011) the nonlinear time scale is taken as the kinetic time scale, which is not appropriate here since $\partial n_k/\partial t$ in (3.2) is evaluated by the dynamic equation instead of the WKE. The ratio of the spectral evolution and linear time scales is given by

$$\rho = \frac{\tau_{nl}}{\tau_{lin}}. \tag{3.3}$$

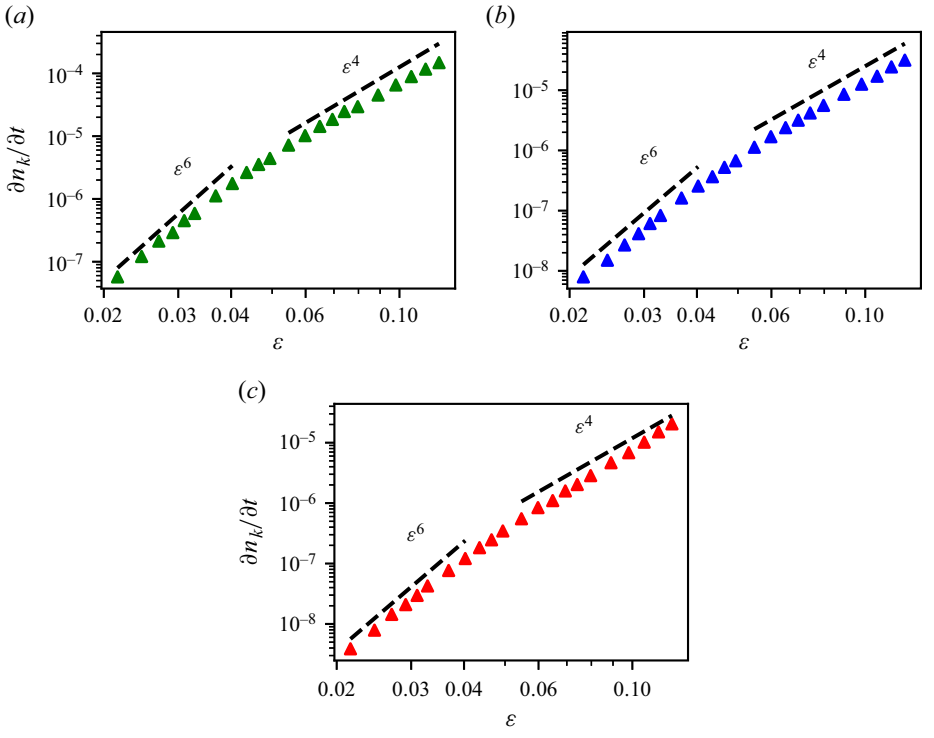

Figure 3. Rate of spectral evolution $\partial n_k/\partial t$ as a function of nonlinearity ε for (*a*) $k = 150$ (green triangles), (*b*) $k = 500$ (blue triangles) and (*c*) $k = 800$ (red triangles), with the kinetic ε^6 and dynamic ε^4 scalings indicated by the dashed lines.

The WKE is expected to be valid only when the time scales are well separated with $\rho \gg O(1)$.

To study the time-scale separation in our cases, we first mention that ρ is, in general, a function of k, as shown in two typical cases in figure 4 for $\Delta\sigma = 0.033$ and 1.461. We see that ρ generally increases with k in a power-law form, which is related to our choice $\beta = 0$ in (2.1) (which makes the nonlinear strength weaker for high k than that from a positive β). Additionally, we see that as $\Delta\sigma$ increases from the former values to the latter, ρ generally drops below $O(1)$, indicating the breakdown of the WKE in the latter case. We next seek to understand the relationship between the time-scale separation and the transition to the dynamic scaling of spectral evolution. To this end, we first note that the transition to dynamic scaling at all inertial-range wavenumbers (see figure 3) occurs at a similar forcing perturbation, indicating that the WKE breaks down for the overall spectral range instead of a particular wavenumber. Therefore, we evaluate ρ at a representative wavenumber $k = 100$, which leads to a relatively low value of ρ in the inertial range as an assessment of the overall validity of wave turbulence theory. We plot in figure 5 $\rho(k = 100)$ as a function of ε, overlaid with the previous plot of $\partial n_k/\partial t$ for $k = 500$ (as an example). We see that the transition to dynamic scaling occurs at $\rho \approx 4 \sim O(1)$, which indicates that the dynamic scaling range is consistent with the failure of the WKE due to the violation of time-scale separation. We also remark that if a different value of k is chosen for the evaluation of ρ, we will end up with a slightly different transition value of ρ which is at most approximately 10 as one can estimate from figure 4.

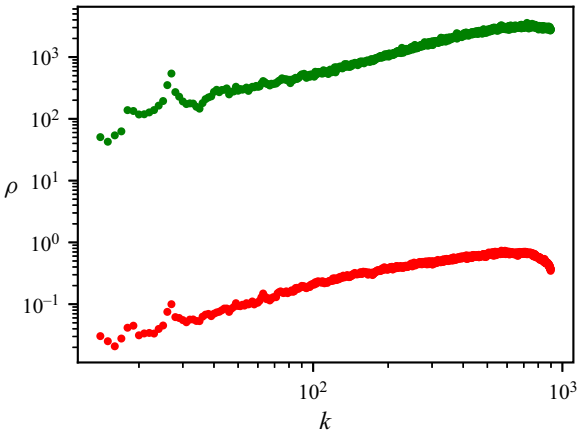

Figure 4. Ratio of time scales ρ as a function of k for cases with $\Delta\sigma = 0.033$, $\varepsilon = 0.022$ (green circles) and $\Delta\sigma = 1.461$, $\varepsilon = 0.124$ (red circles).

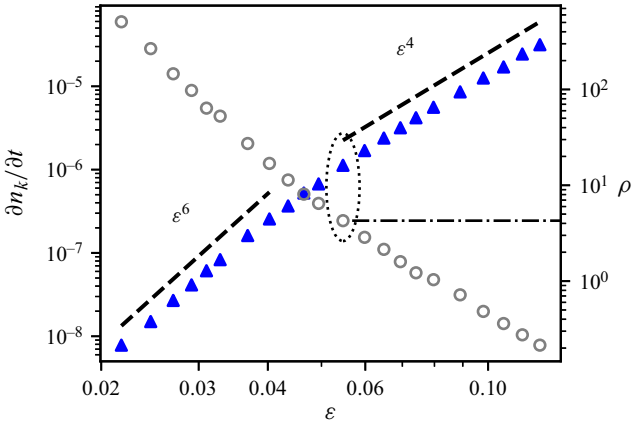

Figure 5. Ratio of the time scales $\partial n_k/\partial t(k = 500)$ (left axis, blue triangles) and $\rho(k = 100)$ (right axis, circles) as functions of ε. The region of transition from kinetic to dynamic scaling is circled, with the corresponding value of ρ indicated (dash-dotted).

While the above analysis reveals the reduction of τ_{nl} as the underlying reason for the transition to dynamic scaling, the cause of this reduction remains unclear. In many previous studies, the reduction of τ_{nl} is attributed to the increase of nonlinearity level, which transits the dynamics into a strong turbulence regime (often associated with intermittency) where the WKE becomes irrelevant. However, we argue that this is not the major reason for the transition to dynamic scaling observed in our study, which is instead mainly triggered by the spectrum being too far from the stationary spectrum after a strong forcing perturbation is applied. To provide evidence for this argument, we repeat our analysis for three additional situations with higher values of ε_0. For each case, we evaluate a transition value ε by the following procedure. We first define a dynamic scaling range as the longest range at a high nonlinearity level where a linear fit of ε^4 has a correlation coefficient $R^2 > 0.998$. The transition value ε is then defined as the leftmost point in the dynamic range. Figure 6 shows that the transition value of ε increases with ε_0 following an approximately linear form of $\varepsilon \sim \varepsilon_0$, and that these transitions all

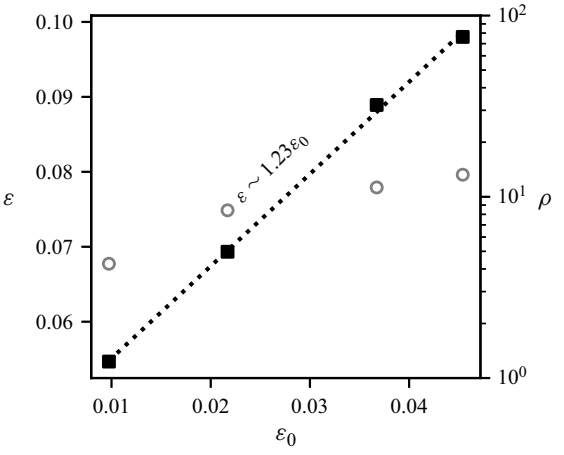

Figure 6. Values of ε (left axis, squares) and $\rho(k = 100)$ (right axis, circles) corresponding to transition to dynamic scaling for each base nonlinearity level ε_0, with a linear fitting (dotted line) and relation indicated.

correspond to $\rho(k = 100) \sim O(1 - 10)$, which is in agreement with the above analysis. This is consistent with the argument about the transition caused by a far-from-stationary spectrum induced by a strong forcing perturbation, since the deviation of the spectrum from the stationary state is approximately measured by the difference between ε and ε_0, which does not change significantly in all cases. Moreover, figure 6 is in clear contradiction with a transition induced by a high nonlinearity level (or strong turbulence), in which case one would otherwise expect that the transition occurs at approximately the same ε for different ε_0.

The failure of the WKE due to the spectrum far from the stationary state can also be reasoned from a thought experiment. Given a spectrum, one can assume *a priori* that the WKE is valid, based on which $\partial n_k/\partial t$ can be computed. Such computed $\partial n_k/\partial t$ may *a posteriori* be found to violate the condition of $\rho \gg O(1)$ that invalidates the assumed WKE. A typical example of this violation has long been known in the Garrett–Munk spectrum of internal gravity waves, where the time-scale separation is not valid in the high-wavenumber/high-frequency portion of the spectrum (e.g. Holloway 1980; McComas & Müller 1981; Lvov, Polzin & Yokoyama 2012; Eden, Pollmann & Olbers 2019; Wu & Pan 2023). In this view, as the spectrum deviates from the stationary state, there exists a critical spectral form (even if the nonlinearity level is relatively low) that drives fast evolution beyond which the WKE fails.

3.2. *Dominant interactions in modal growth*

From § 3.1 we understand that the forcing perturbation (and the associated condensate) creates a deviation of the spectrum from the stationary state, which drives the subsequent spectral evolution. It is therefore reasonable to further argue that the inertial-range modal growth is dominated by direct interaction with the condensate peak, or at least non-local interactions with large-scale features. In this section, we verify this hypothesis using a new set-based interaction analysis. We remark that this is not a trivial task in the sense that these interactions cannot be analysed on the basis of the WKE, but rather must be analysed based on the dynamic equation (2.1) which is valid for all cases.

To start, we first define a set-based modal growth rate $\partial n_k/\partial t|_A$ to be the evolution rate of n_k due to the interaction of mode k with $k_i \in A$ for $i = 1, 2, 3$. By definition, if $A = \Lambda \equiv [-k_{max}, k_{max}]$ (i.e. the full spectral range with $k_{max} = 1024$ after de-aliasing), then $\partial n(k)/\partial t|_A = \partial n(k)/\partial t$. For $A \in \Lambda$, we can compute $\partial n(k)/\partial t|_A$ by invoking (2.1) as

$$\left.\frac{\partial n(k)}{\partial t}\right|_A = \sum_{k_1\in A, k_2\in A, k_3\in A} 2\mathrm{Im}\langle \hat{\psi}_1 \hat{\psi}_2 \hat{\psi}_3^* \hat{\psi}_k^* \rangle \delta_{3k}^{12}, \tag{3.4}$$

where $\delta_{3k}^{12} \equiv \delta(k_1 + k_2 - k - k_3)$ and $\hat{\psi}_k^*$ denotes the complex conjugate of ψ_k. The direct computation of (3.4) in spectral space is very expensive, with a computational complexity of $O(k_{max}^3)$ for each ensemble member of the group at each time instant (the ensemble and the time average are then used to compute the operator $\langle \cdots \rangle$). The computational cost can be significantly reduced if the evaluation of (3.4) can be performed in physical space, which turns out to be possible as we detail in Appendix A, with the result

$$\left.\frac{\partial n(k)}{\partial t}\right|_A \equiv 2\mathrm{Im}\langle \hat{\psi}_k^* \mathcal{F}[B_A(\psi(x))B_A(\psi(x))B_A(\psi^*(x))]\rangle, \tag{3.5}$$

where $\mathcal{F}[\cdots]$ represents the Fourier transform and B_A represents a Fourier-domain filter to select modes in A for a quantity in the physical domain. The computation of (3.5) only requires a number of fast Fourier transforms which is much less expensive than that for (3.4).

In order to sort out the dominant interactions that lead to the growth of a mode k_0, we evaluate $\partial n(k_0)/\partial t|_A$ by setting $A = [-k_{max}, -k_A] \cup [k_A, k_{max}]$ with k_A varying in $[1, k_0]$. Therefore, for fixed k_0, $\partial n(k_0)/\partial t|_A$ can be considered as a function of k_A. As k_A decreases from k_0 to 1, $\partial n(k_0)/\partial t|_A$ accounts for more non-local interactions with large scales (which is more important than interactions with small scales that are not particularly studied in the current setting). Figure 7 plots $\partial n(k_0)/\partial t|_A$ (normalised by $\partial n(k_0)/\partial t$) as a function of k_A for three selected values of k_0 in the inertial range, and for two cases of $\varepsilon = 0.022$ and 0.124 corresponding to regimes of kinetic and dynamic scaling, respectively. We first see that, for each case, the leftmost point (i.e. when $k_A = 1$) recovers the total $\partial n(k_0)/\partial t$, which can be considered as a validation of our computation. For k_A relatively close to k_0, local interactions are represented, with those for higher nonlinearity levels showing stronger fluctuations, i.e. stronger local interactions. Nevertheless, for all cases, there exists a wavenumber k_c (marked in figure 7) at which the normalised $\partial n(k_0)/\partial t|_A$ becomes close to zero or negative. This means that the overall local interactions in the range $[k_c, k_0]$ do not contribute much (or even contribute negatively) to the total $\partial n(k_0)/\partial t$. The major contribution to recover $\partial n(k_0)/\partial t$ occurs for a range immediately left of k_c, where the normalised $\partial n(k_0)/\partial t|_A$ grows quickly from the minimum value to 1. This range features non-local interactions with scale separation of $k_c/k_0 \sim O(0.1)$ (see table 1 for exact numbers) for all cases shown in the figure. The fact that k_c increases with k_0 indicates that the large scales participating in the dominant interactions propagate to higher wavenumbers. For $k_0 = 150$, the non-local interactions mainly involve the forced condensate range up to about $k_c \sim O(10)$. For $k_0 = 500$ and $k_0 = 800$, the small-wavenumber range sufficiently filled with energy during the propagation of the perturbation becomes the dominant interacting modes.

In summary, the analysis here implies that, for all forcing perturbations considered, the inertial-range modal growth is mainly driven by the non-local interactions of the modes with large scales. The local interactions introduce some fluctuations that are stronger for higher-nonlinearity cases, but are sufficiently decayed when enlarging the spectral range

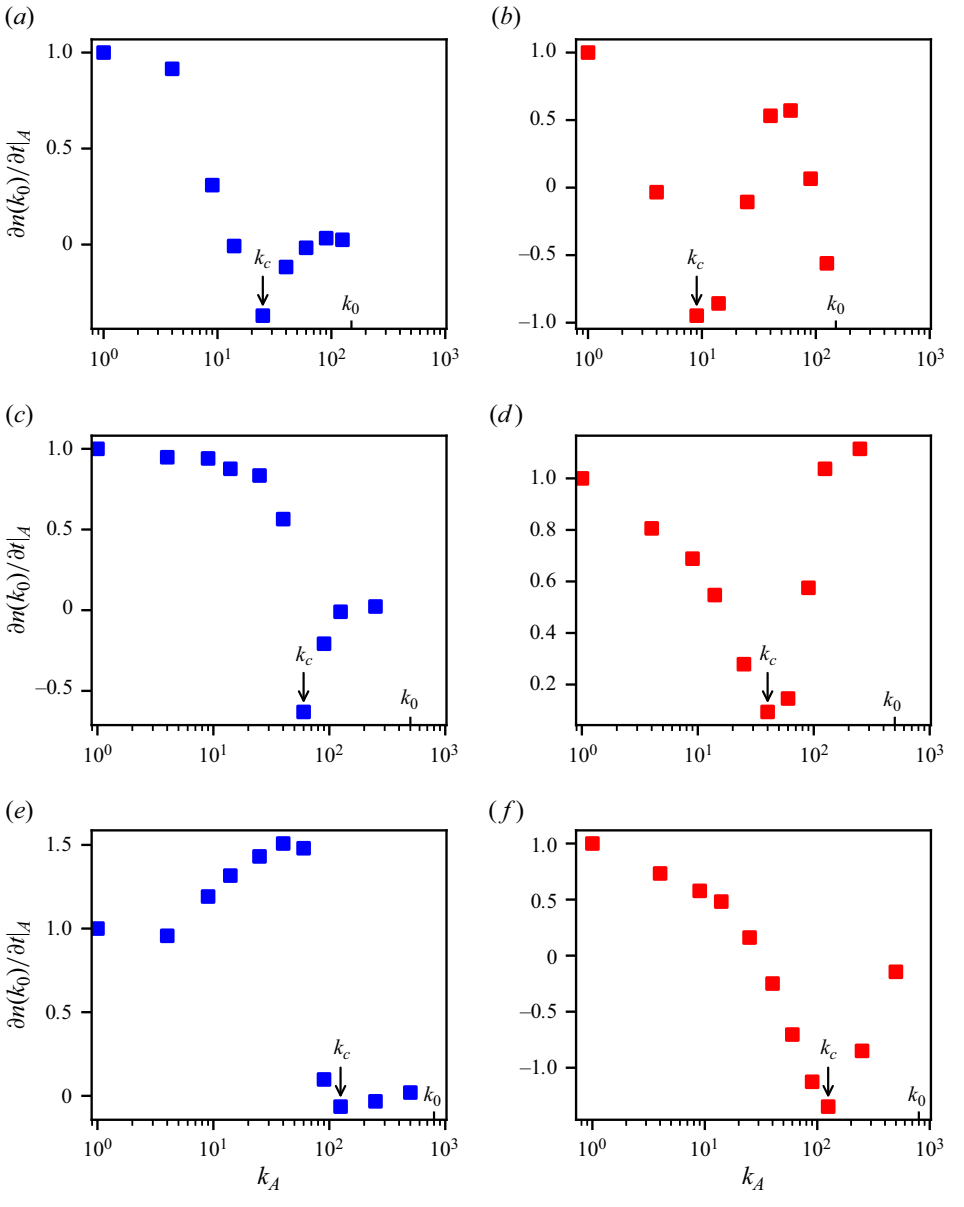

Figure 7. Rate of spectral evolution $\partial n(k_0)/\partial t|_A$, normalised by $\partial n(k_0)/\partial t$, as a function of k_A, for three wavenumbers (a,b) $k_0 = 150$, (c,d) $k_0 = 500$ and (e,f) $k_0 = 800$. The panels on the left (a,c,e) and on the right (b,d,f) are for cases with $\Delta\sigma = 0.033$ and 1.461 in the kinetic and dynamic scaling regimes, respectively. The positions of k_c (where minimum value $\partial n(k_0)/\partial t|_A$ is achieved) and k_0 are indicated in each panel.

around k_0 and before the dominant non-local interactions take place. We also remark that in many situations it is possible to derive a diffusion approximation (assuming the WKE is valid) for non-local interactions as done in McComas & Müller (1981) for three-wave systems and recently in Korotkevich *et al.* (2023) for four-wave systems. However, for a (nonlinear) power-law dispersion relation, the diffusion approximation is only valid for dimension $d \geq 2$, since for $d = 1$ there are no exact resonances when scale-separated

Nonlinearity ε	Wavenumber of interest k_0	Wavenumber at minimum k_c	k_c/k_0
	150	25	0.167
0.022	500	60	0.120
	800	125	0.156
	150	9	0.060
0.124	500	40	0.080
	800	125	0.156

Table 1. Values of k_c and k_c/k_0 for all test cases.

interactions are considered, e.g. for four-wave systems we refer to two large and two small wavenumbers. Therefore, such diffusion approximation is not applicable to our system as far as exact resonances are considered.

4. Conclusion and discussions

In this paper, we numerically study the time scales of spectral evolution of nonlinear waves under perturbed forcing, in order to understand the previously identified 'fast' spectral evolution with the dynamic time scale contradicting the prediction from the WKE. Our study is conducted in the context of the 1-D MMT equation that mimics the wave turbulence of surface gravity waves free of other associated complexities. We show that both kinetic and dynamic time scales can become relevant for spectral evolution depending on the magnitude of the perturbed forcing applied to the stationary spectrum. The kinetic scaling occurs at weaker forcing perturbations, which transits to dynamic scaling as the forcing perturbation becomes strong enough, with the transition corresponding to the situation of the spectral evolution (or nonlinear) time scale dropping to the same level as the linear time scale. Such decrease in nonlinear time scale is mainly induced by the spectrum being far from the stationary state after the forcing perturbation is applied, instead of solely due to the usually considered cause of increasing nonlinearity level. Finally, through a new set-based interaction analysis, we find that the inertial-range spectral growth is dominated by its non-local interactions with the forced condensate or large scales sufficiently filled with energy throughout all nonlinearity levels.

Our study suggests that in assessing the validity of the WKE for transient spectra, the specific spectral forms need to be considered, in conjunction with the traditionally considered factors such as weak/strong turbulence and intermittency. For example, the mechanism understood in this paper may apply to the initial evolution of the wave spectrum, which is sometimes reported to be on the dynamic scale (Dyachenko *et al.* 2003) and sometimes precisely matches the prediction by the WKE (Zhu *et al.* 2022).

In addition, the current results in the MMT model have highlighted mechanisms that have physical relevance in surface gravity waves. We can now expect that in the event that wind forcing provides an adequately strong spectral perturbation and drives the spectrum far from equilibrium, the subsequent spectral evolution may follow the dynamic time scaling instead of prediction from WKE. The growth of spectral energy at small scales in this case should be expected to be governed by their non-local interactions with the forcing peak. Of course there exist many open questions regarding the case for gravity waves, e.g. How strong should the wind forcing and spectral perturbation be to realise dynamic scaling? Does wind direction relative to waves matter in this case? Does the three-wave process that generates bound modes play a role in the spectral evolution of

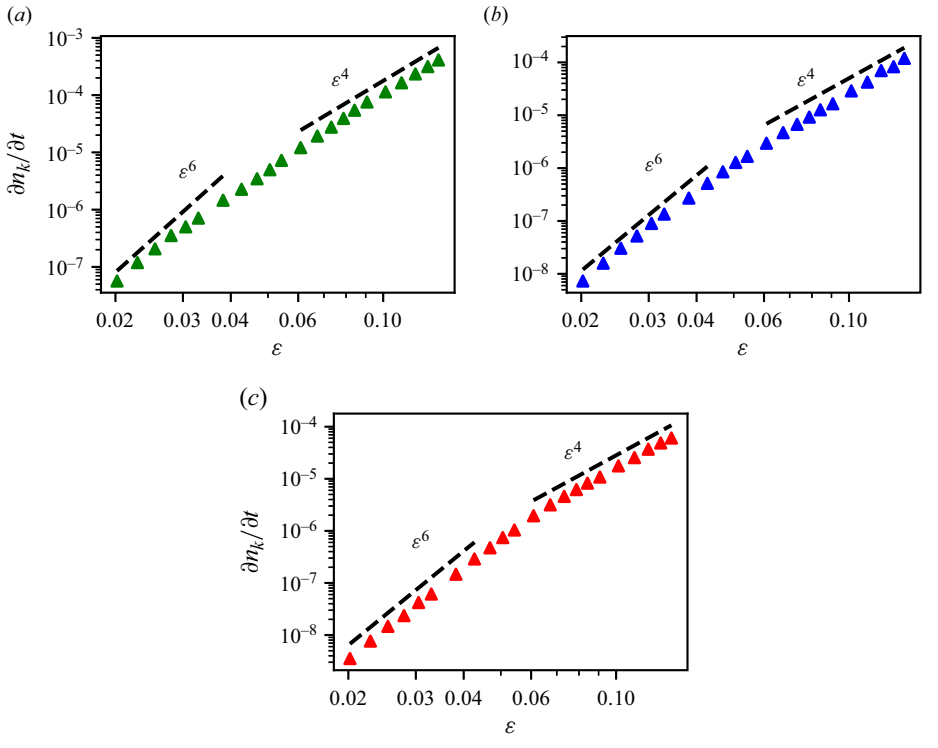

Figure 8. See caption for figure 3, but for the focusing case.

gravity waves? We will consider a future study directly regarding surface gravity waves by applying the methodology developed in this paper, where some of the questions above will be answered.

Acknowledgements. The authors thank Professor M. Onorato for helpful discussions on this work during the Simons Collaboration on Wave Turbulence Annual Meeting in 2022.

Funding. The authors acknowledge the Simons Foundation for funding support for this work.

Declaration of interests. The authors report no conflict of interest.

Author ORCIDs.
Ashleigh Simonis https://orcid.org/0009-0000-3876-8160;
Alexander Hrabski https://orcid.org/0000-0001-9620-5833;
Yulin Pan https://orcid.org/0000-0002-7504-8645.

Appendix A. Fast computation for set-based interaction analysis

We start by reordering (3.4) (by interchanging allowed operations) as

$$\left.\frac{\partial n(k)}{\partial t}\right|_A = 2\mathrm{Im}\langle\hat{\psi}_k^* \sum_{k_1\in A, k_2\in A, k_3\in A} \hat{\psi}_1\hat{\psi}_2\hat{\psi}_3^*\delta_{3k}^{12}\rangle. \tag{A1}$$

The significant computational cost comes from the summation term on the right-hand side of (A1). To reduce the computational cost, we can consider the summation term as the

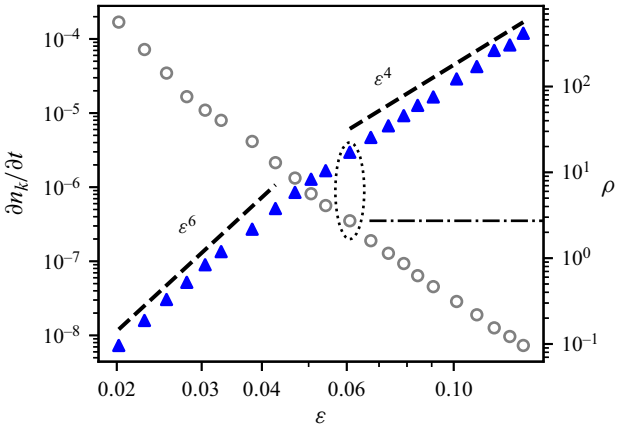

Figure 9. See caption for figure 4, but for the focusing case.

Fourier transform of a physical-space quantity:

$$\sum_{k_1\in A,k_2\in A,k_3\in A} \hat{\psi}_1\hat{\psi}_2\hat{\psi}_3^*\delta_{3k}^{12} = \mathcal{F}[B_A(\psi(x))B_A(\psi(x))B_A(\psi^*(x))], \tag{A2}$$

where $\mathcal{F}[\cdots]$ represents the Fourier transform and B_A represents a Fourier-domain filter to select modes in A for a physical-domain function $\psi(x)$. Equation (A2) can be understood from the convolution theorem for three functions, i.e. spectral-domain convolution is equal to the physical-domain multiplication. One can also directly confirm that this is true by starting from the right-hand side and expressing each $B_A(\psi(x))$ as the summation of Fourier modes:

$$\frac{1}{2\pi}\int \exp(-\mathrm{i}kx)\sum_{k_1\in A}\hat{\psi}(k_1)\exp(\mathrm{i}k_1x)\sum_{k_2\in A}\hat{\psi}(k_2)\exp(\mathrm{i}k_2x)\sum_{k_3\in A}\hat{\psi}^*(k_3)\exp(-\mathrm{i}k_3x)\,\mathrm{d}x, \tag{A3}$$

which can be reorganised as

$$\frac{1}{2\pi}\int \sum_{k_1\in A,k_2\in A,k_3\in A}\hat{\psi}(k_1)\hat{\psi}(k_2)\hat{\psi}^*(k_3)\exp(\mathrm{i}(k_1+k_2-k-k_3)x)\,\mathrm{d}x. \tag{A4}$$

We see that (A4) is the same as the left-hand side of (A1) after considering $(1/2\pi)\int\exp(\mathrm{i}(k_1+k_2-k-k_3)x) = \delta(k_1+k_2-k-k_3)$.

Appendix B. Results from cases with focusing nonlinearity

In this appendix, we summarise results from cases with focusing nonlinearity, i.e. $\lambda=-1$ in (2.1). All other parameters in the study are kept consistent with those in the defocusing cases reported in the main paper. Figures 8 and 9 show respectively the scaling of $\partial n_k/\partial t$ with ε and the study regarding ρ, as counterparts of figures 3 and 4 in the main paper. It is clear from these figures that the main conclusion made for the defocusing case also applies to the focusing case.

References

Annenkov, S.Y. & Shrira, V.I. 2006 Role of non-resonant interactions in the evolution of nonlinear random water wave fields. *J. Fluid Mech.* **561**, 181–207.

Annenkov, S.Y. & Shrira, V.I. 2009 'Fast' nonlinear evolution in wave turbulence. *Phys. Rev. Lett.* **102** (2), 024502.

Annenkov, S.Y. & Shrira, V.I. 2018 Spectral evolution of weakly nonlinear random waves: kinetic description versus direct numerical simulation. *J. Fluid Mech.* **844**, 766–795.

Autard, L. 1995 PhD thesis. Université Aix-Marseille I and II.

Banks, J.W., Buckmaster, T., Korotkevich, A.O., Kovači, G. & Shatah, J. 2022 Direct verification of the kinetic description of wave turbulence for finite-size systems dominated by interactions among groups of six waves. *Phys. Rev. Lett.* **129** (3), 034101.

Buckmaster, T., Germain, P., Hani, Z. & Shatah, J. 2021 Onset of the wave turbulence description of the longtime behavior of the nonlinear Schrödinger equation. *Invent. Math.* **225** (3), 787–855.

Cai, D., Majda, A.J., McLaughlin, D.W. & Tabak, E.G. 1999 Spectral bifurcations in dispersive wave turbulence. *Proc. Natl Acad. Sci. USA* **96** (25), 14216–14221.

Cai, D., Majda, A.J., McLaughlin, D.W. & Tabak, E.G. 2001 Dispersive wave turbulence in one dimension. *Physica* D **152**, 551–572.

Chibbaro, S., De Lillo, F. & Onoroto, M. 2017 Weak versus strong wave turbulence in the Majda-McLaughlin-Tabak model. *Phys. Rev. Fluids* **2** (5), 052607.

Deng, Y. & Hani, Z. 2021 On the derivation of the wave kinetic equation for NLS. *Forum Maths Pi* **9**, e6.

Deng, Y. & Hani, Z. 2023 Full derivation of the wave kinetic equation. *Invent. Math.* **233** (2), 543–724.

Dyachenko, K.B., Trulsen, K., Krogstad, H.E. & Socquet-Juglard, V.E. 2003 Evolution of a narrow-band spectrum of random surface gravity waves. *J. Fluid Mech.* **478**, 1–10.

Eden, C., Pollmann, F. & Olbers, D. 2019 Numerical evaluation of energy transfers in internal gravity wave spectra of the ocean. *J. Phys. Oceanogr.* **49** (3), 737–749.

Falcon, E. & Mordant, N. 2022 Experiments in surface gravity-capillary wave turbulence. *Annu. Rev. Fluid Mech.* **54**, 1–25.

Galtier, S., Nazarenko, S., Newell, A.C. & Pouquet, A. 2000 A weak turbulence theory for incompressible magnetohydrodynamics. *J. Plasma Phys.* **63** (5), 447–488.

Hasselmann, K. 1962 On the non-linear energy transfer in a gravity-wave spectrum. Part I. General theory. *J. Fluid Mech.* **12**, 481–500.

Holloway, G. 1980 Oceanic internal waves are not weak waves. *J. Phys. Oceanogr.* **10** (6), 906–914.

Hrabski, A. & Pan, Y. 2020 Effect of discrete resonant manifold structure on discrete wave turbulence. *Phys. Rev.* E **102** (4), 041101.

Hrabski, A. & Pan, Y. 2022 On the properties of energy flux in wave turbulence. *J. Fluid Mech.* **936**, A47.

Janssen, P. 2004 *The Interaction of Ocean Waves and Wind*. European Centre for Medium-Range Weather Forecasts. Cambridge University Press.

Korotkevich, A.O., Nazarenko, S.V., Pan, Y. & Shatah, J. 2023 Nonlocal gravity wave turbulence in presence of condensate. arXiv:2305.01930.

Lvov, Y.V., Polzin, K.L. & Yokoyama, N. 2012 Resonant and near-resonant internal wave interactions. *J. Phys. Oceanogr.* **42** (5), 669–691.

L'vov, V.S., L'vov, Y., Newell, A.C. & Zakharov, V.E. 1997 Statistical description of acoustic turbulence. *Phys. Rev.* E **56** (1), 390–405.

L'vov, V.S. & Nazarenko, S. 2010 Discrete and mesoscopic regimes of finite-size wave turbulence. *Phys. Rev* E **82** (5), 056322.

Majda, A.J., McLaughlin, D.W. & Tabak, E.G. 1997 A one-dimensional model for dispersive wave turbulence. *J. Nonlinear Sci.* **7** (1), 9–44.

McComas, C.H. & Müller, P. 1981 Time scales of resonant interactions among oceanic internal waves. *J. Phys. Oceanogr.* **11** (2), 139–147.

Nazarenko, S. 2011 *Wave Turbulence*. Lecture Notes in Physics. Springer.

Nazarenko, S. & Lukaschuk, S. 2016 Wave turbulence on water surface. *Annu. Rev. Condens. Mat. Phys.* **7**, 61–88.

Nazarenko, S. & Onorato, M. 2006 Wave turbulence and vortices in Bose-Einstein condensation. *Physica* D **219** (1), 1–12.

Newell, A.C., Nazarenko, S. & Biven, L. 2006 Wave turbuelnce and intermittency. *Physica* D **152**, 520–550.

Newell, A.C. & Rumpf, B. 2011 Wave turbulence. *Annu. Rev. Fluid Mech.* **43**, 59–78.

Onorato, M., Osborne, A.R., Serio, M., Resio, D., Pushkarev, A., Zakharov, V.E. & Brandini, C. 2002 Freely decaying weak turbulence for sea gravity waves. *Phys. Rev. Lett.* **89** (14), 144051.

PAN, Y. & YUE, D.K.P. 2014 Direct numerical investigation of capillary waves. *Phys. Rev. Lett.* **113** (9), 094501.

RUMPF, B. & NEWELL, A.C. 2013 Wave instability under short-wave amplitude modulations. *Phys. Lett.* A **377** (18), 1260–1263.

RUMPF, B, NEWELL, A.C. & ZAKHAROV, V.E. 2009 Turbulent transfer of energy by radiating pulses. *Phys. Rev. Lett.* **103** (7), 074502.

RUMPF, B. & SHEFFIELD, T.Y. 2015 Transition of weak wave turbulence to wave turbulence with intermittent collapses. *Phys. Rev* E **92** (2), 1539–3755

TANAKA, M. 2001 Verification of Hasselmann's energy transfer among surface gravity waves by direct numerical simulations of primitive equations. *J. Fluid Mech.* **28**, 41–60.

VAN VLEDDER, G.P. & HOLTHUIJSEN, L.H. 1993 The directional response of ocean waves to turning winds. *J. Phys. Oceanogr.* **23** (2), 177–192.

WASEDA, T., TOBA, Y. & TULIN, M.P. 2001 Adjustment of wind waves to sudden changes of wind speed. *J. Phys. Oceanogr.* **57**, 519–533.

WU, Y. & PAN, Y. 2023 Energy cascade in the Garrett-Munk spectrum of internal gravity waves. *J. Fluid Mech.* **975**, A11.

ZAKHAROV, V.E. 1968 Stability of periodic waves of finite amplitude on the surface of a deep fluid. *J. Appl. Mech. Tech. Phys.* **9** (2), 190–194.

ZAKHAROV, V.E. & FILONENKO, N.N. 1967 Weak turbulence of capillary waves. *J. Appl. Mech. Tech. Phys.* **8** (5), 37–40.

ZAKHAROV, V.E., PUSHKAREV, A.N. & DIAS, F. 2001 One-dimensional wave turbulence. *Phys. Rep.* **398** (1), 1–65.

ZHANG, Z. & PAN, Y. 2022*a* Numerical investigation of turbulence of surface gravity waves. *J. Fluid Mech.* **933**, A58.

ZHANG, Z. & PAN, Y. 2022*b* Forward and inverse cascades by exact resonances in surface gravity waves. *Phys. Rev.* E **106** (4), 044213.

ZHU, Y., SEMISALOV, B., KRSTULOVIC, G. & NAZARENKO, S. 2022 Testing wave turbulence theory for the Gross-Pitaevskii system. *Phys. Rev.* E **106** (1), 014205.

ZHU, Y., SEMISALOV, B., KRSTULOVIC, G. & NAZARENKO, S. 2023 Direct and inverse cascades in turbulent Bose-Einstein condensates. *Phys. Rev. Lett.* **130** (13), 13301.